Targeted intracellular delivery to hypoxic human breast cancer stem cells

Makela, Ashley V[1], Tundo, Anthony[1], Liu, Huiping[2], Hermiston, Terry[3], Contag, Christopher, H[1,4*]

[1]Institute for Quantitative Health Science and Engineering, Michigan State University, East Lansing MI
[2]Department of Pharmacology and Medicine, Northwestern University Feinberg School of Medicine, Chicago, IL
[3] GLAdiator BioSciences, Mill Valley, CA
[4] Departments of Biomedical Engineering, and Microbiology, Genetics, and Immunology, Michigan State University, East Lansing MI
*corresponding author

Keywords: cancer stem cells, hypoxia, phosphatidylserine, protein S, patient derived xenograft

Abstract

Cancer stem cells (CSCs) comprise the root of cancers and remain a therapeutic challenge since they are quiescent, resist traditional therapies and are fundamentally tumorigenic. Therefore, effective cancer treatments require CSC-targeted approaches that function in representative CSC microenvironments. CSCs exhibit few distinguishable and targetable characteristics, however phosphatidylserine (PS) exposure on the cell surface and localization to hypoxic regions of the tumor are speculated traits. We have reported that a truncated protein S (GlaS) binds PS and is internalized, enabling intracellular delivery of molecular payloads. GlaS delivery was evaluated in patient-derived CD44+ mammary CSCs under different oxygen concentrations. A higher percentage of CD44+GlaS+ cells were observed in hypoxia compared to cells in physoxia or hyperoxia that tracked to small CD44+ cells, which are likely aggressive tumorigenic CSCs. Delivery of therapeutics to the cytoplasm of CSCs will enable new therapies directed at intracellular targets, ultimately eliminating CSCs.

Introduction

Although there have been significant advancements in breast cancer therapy, challenges still persist, especially in the treatment of breast cancer stem cells (CSC). CSC are functionally defined with self-renewal and tumorigenic properties, often quiescent, can undergo differentiation, and have been shown to be a source of metastasis[1–4]. CSCs tend to be localized in hard-to-reach hypoxic regions of the tumor; all of these characteristics render CSC resistant to traditional therapies (*i.e.*, chemotherapy, radiation therapy, and certain molecular targeted drugs). Residual disease is likely due to conventional therapies failing to eliminate CSC concurrently with the bulk of the tumor, allowing the CSC to persist and subsequently relapse, differentiate and metastasize. The necessity to eliminate CSC is paramount for effective treatment and methods for targeting the CSC population are essential. However, CSCs exhibit few characteristics that allow them to be distinguished and targeted. CSC characteristics that are relevant and to be targeted in this study include outer leaflet phosphatidylserine (PS) exposure on the surface[5], CD44 expression[6], and a tendency to reside in the hypoxic tumor microenvironment (TME)[6].

PS is a negatively charged glycerophospholipid present in all eukaryotic cell membranes. In most physiologically healthy cells, PS is preferentially located on the inner leaflet of the plasma membrane due to the action of ATP-dependent aminophospholilpid flippase[7]. The externalization of PS is observed under some biological processes including apoptosis[8], blood coagulation[9], disease[10,11] and on stem cells[12]. Dying cells expose PS on their surface and are subsequently eliminated or cleared by immune cells; PS externalization signals the immune system not to mount an immune response to the antigens on cells with self markers to avoid autoimmune responses. As such tumor cells, that have increased PS on their outer membrane[10,11] and high expression of CD47[13] evade immune destruction. PS externalized on cancer cells provides an immunosuppressive mechanism, facilitating tumor growth and enabling metastasis[14–16]. PS-binding proteins (*i.e.*, Annexin V; AnnV)[17,18] and mAbs (*i.e.,* Bavituxumab; Bavi)[19] are being studied as a means of targeting PS-expressing cells. Bavi works to reverse the immunosuppressive actions of the externalized PS[20], acting as an immunomodulatory therapy; although these proteins bind to PS on the cell surface, they are not internalized, limiting their use to the delivery of surface-active agents. In contrast, we have found that a truncated protein S comprised of the PS-binding γ-carboxyglutamate (Gla) domain and four epidermal growth factor (EGF) domains (collectively referred to as GlaS), binds PS on the outer leaflet and is internalized after binding[21] enabling delivery of payloads to the cytoplasm of cells with externalized PS which would include those in the hypoxic regions of tumors.

Hypoxia is common within solid tumors, and in the context of breast tumors, can be as low as 1% O_2 (severe hypoxia), compared to physoxia, which is oxygen found in normal tissue, at 3-7% O_2[22] whereas cells in culture are typically propagated at 21% O_2. Further, the stem cell niche also operates under reduced oxygen conditions of 2-6% O_2[23]. Hypoxia inducible factors (HIFs) are two transcription factors (HIF1α and HIF2α) that are expressed upon cellular exposure to decreased O_2, and their activity regulates the expression of many stem cell markers[24–26]. In addition, hypoxia combined with radiotherapy seems to enhance the stem-like properties of these cells[27]. In the context of this study, the experimental oxygen levels were 7% for physoxia and 4% for hypoxia (mild). Typically, studies of CSC utilize cell culture conditions at room oxygen levels (21%) and

control oxidative stress by adding antioxidants to the media[28]. However, no cells in internal organs, with the exception of cells lining the alveoli in the lungs, grow in 21% oxygen, and in the tumor microenvironment the oxygen levels can be very low. These discrepancies in oxygen concentrations in culture verses oxygen levels in tissues, can potentially lead to erroneous results when investigating cellular characteristics and responses to investigative therapeutics[29,30]. Consequently, it is essential to study CSC under conditions that approximate their niche in the tumor microenvironment, specifically with regard to oxygen levels.

This study examines the effects of oxygen conditions on the targeted binding and internalization of the protein, GlaS, in CSC derived from triple-negative human breast cancer patients as marked by CD44 protein expression on lineage negative tumor cells. We show that there is increased PS externalization on CSC when cultured in hypoxic conditions (4%) relative to physioxia (7%) and hyperoxia (21%), and that there are more CD44+GlaS+ cells by flow cytometry in hypoxia. Further, a fraction of small-sized CD44+ cells have increased levels of GlaS staining, suggesting that the GlaS may more effectively target a subset of more highly stem-like, quiescent and tumorigenic CSC.

Results

Frequency of CD44+ cells and CD44+GlaS+ cells at three oxygen concentrations

Breast cancer patient-derived CD44+ CSCs could not be maintained in culture and were therefore propagated in NSG mice as human patient-derived xenografts (PDXs). Five PDX lines - M1L2T, M2L2T, M3L2G, CTC205 (L2T) and CTC092 (L2T) - were evaluated. The M1 was derived from pleural effusion metastasis and M2 and M3 of human breast tumors[31] and CTC205 and CTC092 were derived from circulating tumor cells of patients with breast cancer[32,33]. The L2T refers to labeling with the Luc2-tdTomato reporter, and L2G to labeling with the Luc2-eGFP[31]. The PDX tumors had variable growth rates in mice, and the lines M1L2T and CTC205 grew the fastest, followed by M2L2T and M3L2G, and CTC092, respectively. After the cells were harvested from dissociated tumor tissue they were placed in hypoxic (4%), physoxic (7%) or hyperoxic (21%) conditions overnight. Following overnight culture, the percent of CD44+ cells from each PDX tumor varied slightly, although none had significant differences in the percent of CD44+ cells under different oxygen conditions; there was an average of 62% CD44+ cells in hypoxic, 64% in physoxic and 60% in hyperoxic conditions ($F_{2,36}$=1.32, p=.28) from live cells (**Fig. 1a,d**). Within populations there were no differences in the frequency of CD44+ cells (**Supplementary Fig. 1**) between the oxygen conditions in M1L2T ($F_{2,6}$=4.89, p=.055), M2L2T ($F_{2,5}$=2.13, p=.21), M3L2G ($F_{2,6}$=2.26, p=.19) and CTC092 ($F_{2,1}$=56.2, p=.09) cells. However, there were differences in the frequency of CD44+ cells in populations held at different oxygen conditions for the CTC205 ($F_{2,6}$=11.96, p=.008) cells, with lower percentages of CD44+ cells in the hyperoxic condition vs the hypoxic (p=.049) and physoxic (p=.007) conditions. Despite negligible differences in the frequency of CD44+ cells in the three oxygen concentrations, the frequency of CD44+GlaS+ cells did vary with oxygen concentration.

The percent of GlaS+ cells from the live CD44+ population (CD44+GlaS+, **Fig. 1b,e**) were significantly different among all the PDX cell lines at different oxygen conditions ($F_{2,36}$=27.69, p<.0001). CD44+GlaS+ frequencies were increased in hypoxic (61%) vs physoxic (47%; p=.01) and hyperoxic (28%; p<.0001) conditions. The percent of CD44+GlaS+ cells was also significantly increased in the physoxic vs the hyperoxic condition (p=.0003). Within a given PDX line, there were significant differences in the frequency of CD44+GlaS+ cells (**Supplementary Fig. 2**) in M1L2T ($F_{2,6}$=67.88, p<.0001), M2L2T (p=.01) and M3L2G ($F_{2,6}$=37.01, p=.0004) cells. There were no differences in the frequency of CD44+GlaS+ cells in CTC092 ($F_{2,1}$=3.85, p=.34) and CTC205 ($F_{2,6}$=1.8, p=.25) lines. The percentages of GlaS+ cells in the CD44- population (**Fig. 1c,f**) between oxygen conditions were not significantly different (p=.054).

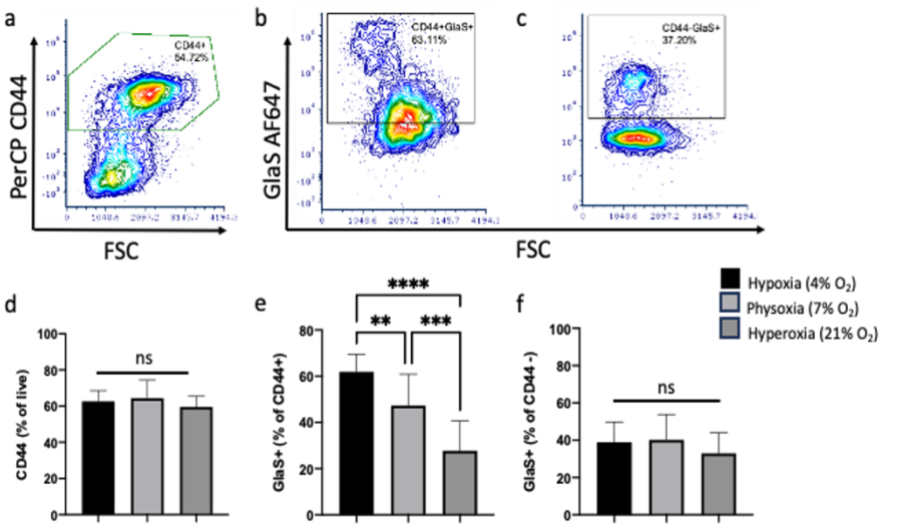

Figure 1. GlaS binding to CD44+ cells is increased in hypoxia. Flow cytometry dot plots of representative (hypoxic) CD44+ (**a**; from live), CD44+GlaS+ (**b**) and CD44-GlaS+ (**c**) populations. No significant difference was found in CD44+ populations between oxygen conditions (**d**). There was significantly more CD44+GlaS+ cells in hypoxic vs physoxic and hyperoxic conditions, and physoxic vs hyperoxic conditions (**e**). There was no significant difference in CD44-GlaS+ populations between oxygen conditions (**f**). n=13 per O^2 concentration (n=5 PDX tumor types, n=1-3 technical replicates). **p<.01, ***p<.001, ****p<.0001, ns=not significant

The population of smaller-sized CD44+ cells had greater intensity of GlaS staining

From the CD44+ cells, there were two populations which could be distinguished by their size (as determined by forward scatter; FSC) and GlaS staining intensity (as determined by median fluorescence intensity, MFI; **Fig. 2**). The cells with higher FSC (larger) had decreased GlaS MFI ($GlaS^{low}$large) vs a population with lower FSC and increased GlaS MFI ($GlaS^{high}$small). $GlaS^{low}$large cells had lower GlaS binding (**Fig. 2b,e**) and were 1.5x larger (**Fig. 2c,f**) versus the $GlaS^{high}$small cells (p<.0001 in all oxygen conditions for FSC (t(24)=13.49; hypoxic, t(24)=9.58; physoxic and t(16.54)=9.72; hyperoxic) and GlaS MFI (t(12.05)=10.45; hypoxic and t(12.11)=10.47; hyperoxic)). GlaS MFI was 21x, 18x and 10x higher in the smaller vs larger CD44+ population at hypoxic, physoxic and hyperoxic conditions, respectively. Differences in GlaS MFI relative to oxygen conditions were apparent in the $GlaS^{high}$small population (p=.0008), but not in the $GlaS^{low}$large population ($F_{2,36}$=1.63, p=0.21). Further, CD44 MFI was also different in these two populations; cells which were cultured in physoxic (p<.0001) and hyperoxic (p<.0001) conditions had a higher CD44 MFI in the $GlaS^{low}$large vs the $GlaS^{high}$small population. There were no significant differences

in CD44 MFI in the GlaS^{low}large vs GlaS^{high}small populations in cells cultured under hypoxic conditions (t(16.32)=1.8, *p*=.09).

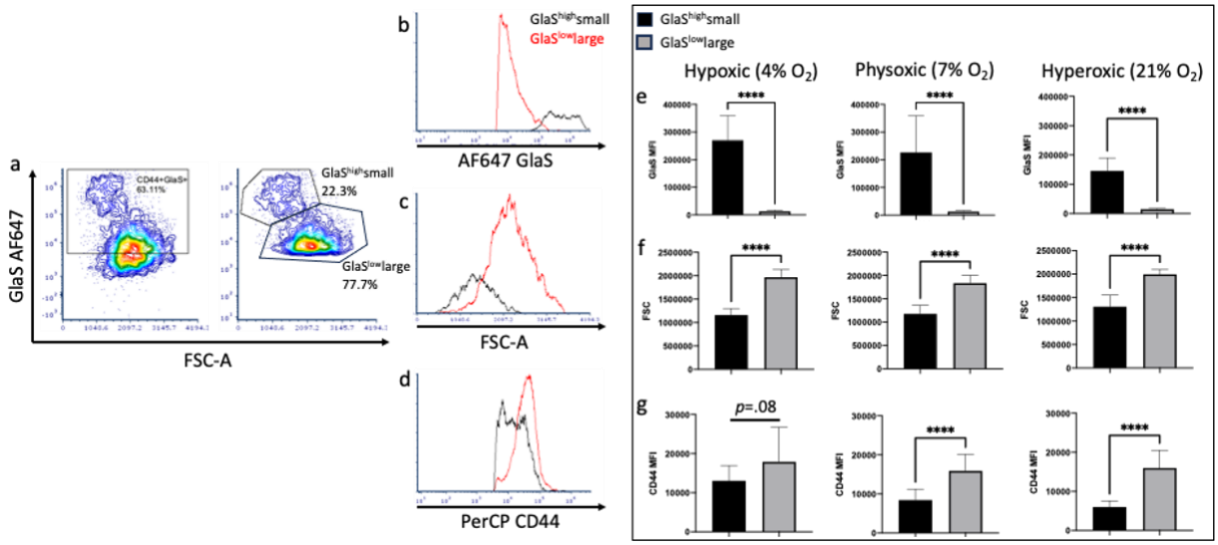

Figure 2. There are two populations of CD44+ cells with different sizes, GlaS binding and CD44 expression. Dot plots of flow cytometry data demonstrate that there are CD44+GlaS+, GlaS^{high}small and GlaS^{low}large populations of cells (**a**). Flow cytometry histograms demonstrate AF647 GlaS MFI (**b**), FSC-A (**c**) and PerCP CD44 MFI (**d**) for GlaS^{high} (black) and GlaS^{low} (red) populations. AF647 GlaS MFI (e), FSC-A (f) and PerCP CD44 MFI (g) are quantified for GlaS^{high}small and GlaS^{low}large populations of cells in hypoxic, physoxic and hyperoxic conditions. n=13 (n=5 PDX tumor types, n=1-3 technical replicates). ****p<.0001

Although the overall CD44+ population did not change between oxygen conditions, there was a difference in CD44 levels (MFI) when considering the GlaS^{low}large and GlaS^{high}small populations. Oxygen condition only had an effect on CD44 MFI in the GlaS^{high}small population ($F_{2,36}$=19.74, *p*<.0001, **Fig. 3a,c**), with increased CD44 MFI in the cells cultured in hypoxic conditions vs those cultured in physoxic (*p*=.007) and hyperoxic (*p*<.0001) conditions. Oxygen did not have an effect on the CD44 MFI in the GlaS^{low}large cell population (*p*=.96, **Fig. 3b,d**).

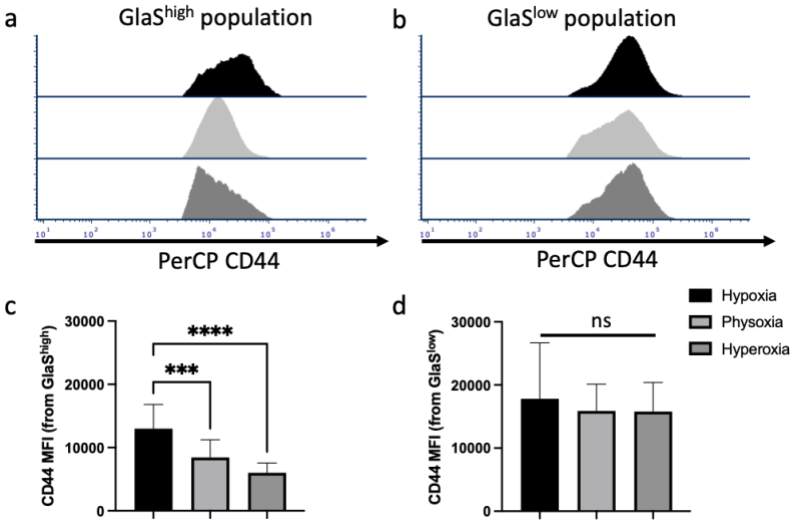

Figure 3. CD44 expression is increased under hypoxia in GlaS^{high}small but not GlaS^{low}large population. Flow cytometry histograms demonstrate median fluorescence intensity (MFI) of PerCP CD44 for GlaS^{high}small (**a**) and GlaS^{low}large (**b**) populations.

CD44 MFI was increased in cells cultured in hypoxic vs physoxic and hyperoxic conditions for GlaS^{high}small population (**c**). There was no significant difference in CD44 MFI under any oxygen condition for the GlaS^{low}large population. n=13 per O^2 concentration (n=5 PDX tumor types, n=1-3 technical replicates). ***p<.001, ****p<.0001, ns=not significant

PS-binding by Annexin V, Antibody 11.31 and Bavituximab on CD44+ cells

Differences in PS-binding of Annexin V (AnnV), the antibodies, 11.31 and Bavituximab (Bavi), on CD44+ cells were also observed when cells were held at the different oxygen conditions **(Fig. 4)**. There was a significant difference in AnnV staining among all oxygen conditions ($F_{2,36}$=9.78, p=.0004, **Fig. 4d**); specifically, there was significantly more CD44+AnnV+ cells in hypoxic (58%) vs physoxic (37%, p=.007) and hypoxic vs hyperoxic (32%, p=.0005) conditions. The antibody 11.31 also demonstrated differences in binding between oxygen conditions (p=.0009, $F_{2,12}$=13.17, **Fig. 4e**) with an increased frequency of CD44+11.31+ cells in hypoxic (56%) vs hyperoxic (11%, p=.0007) and physoxic (39%) vs hyperoxic (p=.02) conditions. Bavi binding followed the same trend, with significant differences between all oxygen conditions ($F_{2,8}$=8.3, p=.01, **Fig. 4f**) with increased CD44+Bavi+ cells in hypoxic (81%) vs hyperoxic (45%, p=.01) conditions.

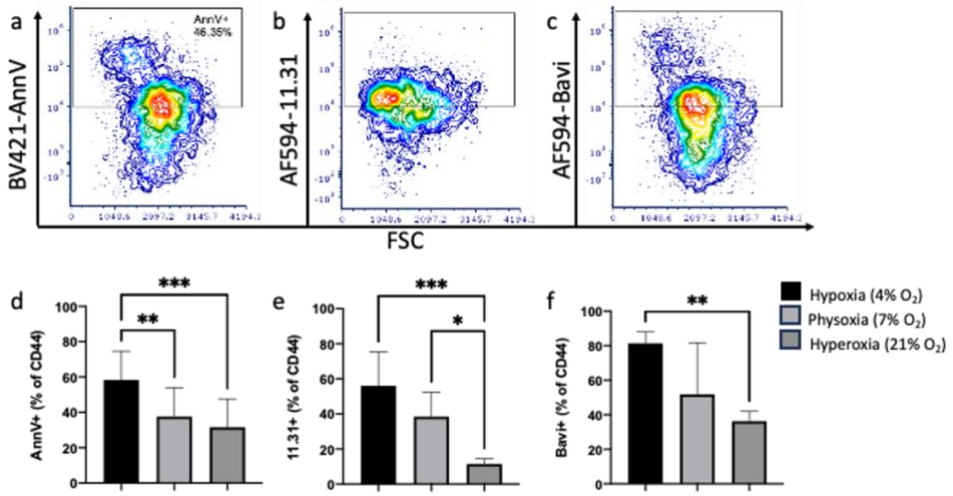

Figure 4. PS-binding by Annexin V, Bavituximab and 11.31 are increased in CD44+ cells in hypoxia. Flow cytometry dot plots of representative (hypoxic) CD44+AnnV+ (**a**), CD44+11.31+ (**b**) and CD44+Bavi+ (**c**) populations. Cells cultured in hypoxic conditions had significantly more AnnV+ (**d**), 11.31+ (**e**) and Bavi+ (**f**) staining vs cells which were cultured in hyperoxic conditions. There was more CD44+AnnV+ cells in hypoxic vs physoxic conditions and more CD44+11.31+ cells in physoxic vs hyperoxic conditions. AnnV; n=13 per O^2 concentration (n=5 PDX tumor types, n=1-3 technical replicates), Bavi/11.31; n=3-5 per O^2 concentration (n=3-5 PDX tumor types, n=1 technical replicate). *p<.05, **p<.01, ***p<.001

Although GlaS, AnnV and the PS control antibodies (Bavi and 11.31) all target PS, there were some differences in staining for these four proteins on the PDX lines (**Fig. 5**). There were significant differences in PS staining under hypoxic conditions ($F_{3,31}$=3.57, p=.025, **Fig. 5a**) with more CD44+Bavi+ cells than CD44+AnnV+ (p=.023) and CD44+11.31+ (p=.035). PS staining was also different among cells cultured under hyperoxic conditions ($F_{3,31}$=3.6, p=.024, **Fig. 5e)** with the frequency of CD44+11.31+ decreased compared to CD44+AnnV+ (p=.029) and CD44+Bavi+ (p=.036). There were no significant differences among any of the markers in physoxic conditions ($F_{3,30}$=1.19, p=.331, **Fig. 5c**). The percentage of CD44+GlaS+ cells were not different from any of the control PS stains under any of the oxygen conditions. However, we observed that GlaS, AnnV and the PS-binding Abs were not always associated with the same cells (**Fig. 5**). The percentage of CD44+ cells which were GlaS+, AnnV+ and PS control+ (Bavi or 11.31) were 35%, 22% and 9%

for hypoxic (**Fig. 5b**), physoxic (**Fig. 5d**) and hyperoxic (**Fig. 5f**) conditions, respectively. The remaining cells were GlaS+AnnV+PS control- (9%, 5% and 11%), GlaS+PS control+AnnV- (12%, 12% and 2%), AnnV+PS control+GlaS- (9%, 4% and 2%), GlaS only (6%, 8% and 6%), PS control only (12%, 10% and 7%) and AnnV only (5%, 7% and 9%), for hypoxia, physoxia and hyperoxia, respectively. Overall, the percentages of unstained cells increased as oxygen levels increased (13%, 32% and 54%) for hypoxia, physoxia and hyperoxia, respectively, suggesting that there was a decrease in PS expression as oxygen levels increased resulting in lower PS-associated staining.

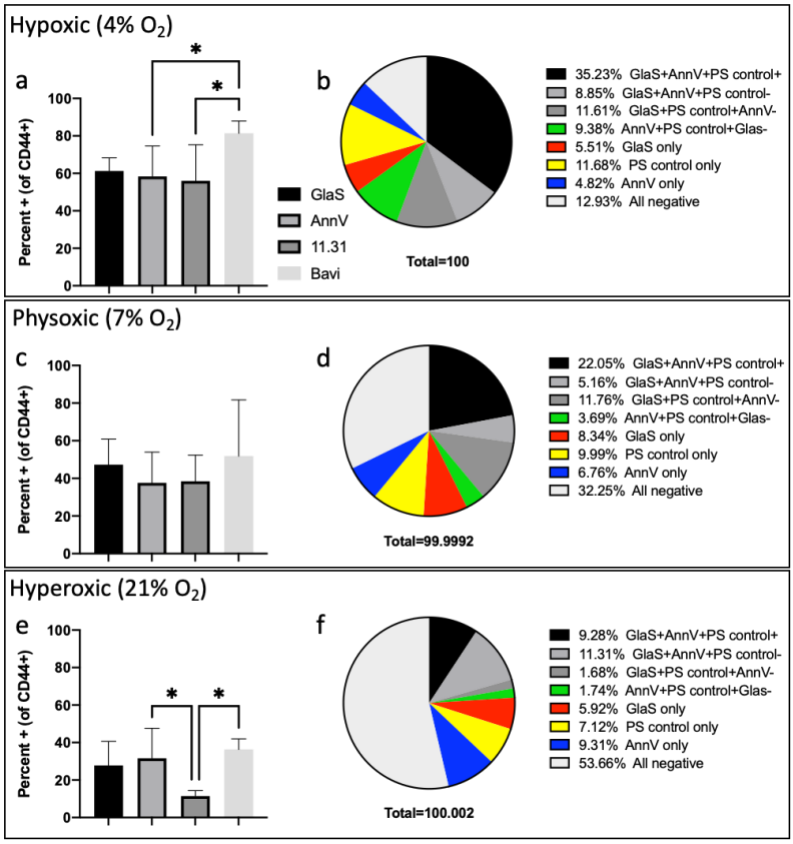

Figure 5 Differences in PS-binding GlaS, Annexin V and PS control Abs. In hypoxic conditions, there was an increase in CD44+Bavi+ compared to CD44+AnnV+ and CD44+11.31+ cells (**a**). No difference in PS staining was observed for cells cultured under physoxic conditions (**c**). In hyperoxic conditions, CD44+11.31+ cells were decreased compared to CD44+AnnV+ and CD44+Bavi+ cells (**e**). Percent of cells with variations of GlaS, AnnV or PS control Ab staining are demonstrated for hypoxia (**b**), physoxia (**d**) and hyperoxia (**f**). AnnV; n=13 per O^2 concentration (n=5 PDX tumor types, n=1-3 technical replicates), Bavi/11.31; n=3-5 per O^2 concentration (n=3-5 PDX tumor types, n=1 technical replicate). *p<.05

Confocal microscopy localizes GlaS to the cytoplasm of PDX derived cells

Microscopy revealed localization of GlaS within isolated PDX-derived cells was different from PS staining controls. When cells are held at hypoxic conditions, GlaS was found both on the membrane of cells as well as within the cells (**Fig. 6, section (S)17 and Supplemental Movie 1**). AnnV (blue arrowhead; **Fig. 6, S11**) and Bavi (yellow arrowhead; **Fig. 6, S15**) were only detected along the membrane of the cells.

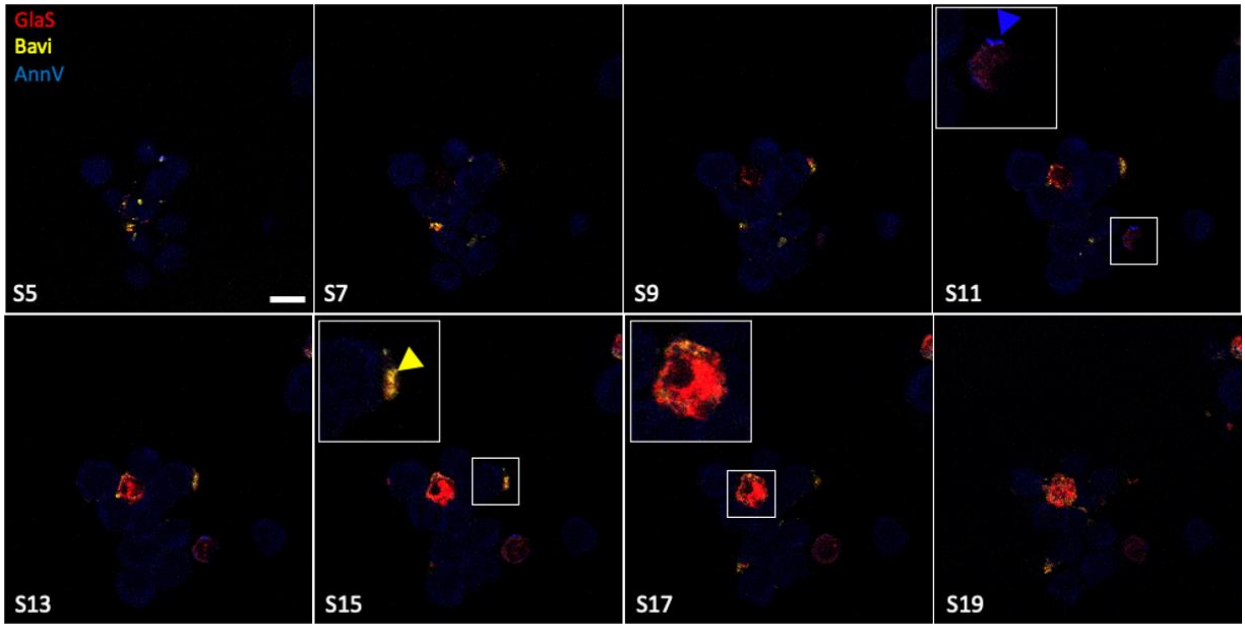

Figure 6. Confocal microscopy of PDX cells reveals intracellular GlaS and cell membrane-bound PS-binding AnnV and Bavi. PDX tumor (M1L2T) was excised from a mouse, dissociated into a single cell suspension and culture overnight at 4% O_2. Cells were stained with AF647 GlaS (red), AF594 Bavi (yellow) and BV421 Annexin V (blue). Zoomed inset (Section(S)11, S15 and S17). Scale bar = 20 μm.

Discussion

The cellular characteristics and location within the hypoxic regions of the TME allow CSCs to evade traditional therapeutics and perpetuate tumor growth. As such, novel therapeutics need to be developed to eliminate CSC where they reside. PS exposure has been identified previously on stem cells[12], as well as healthy vascular endothelial cells, where increased PS externalization was observed after cells were exposed to hypoxic conditions[34]. In the present study, we observed more PS externalization on CSCs under hypoxic conditions and consequently increased GlaS binding and internalization into cells. Because CSCs reside within low oxygen environments *in vivo*, it was anticipated that there would be increased PS externalization when compared to other regions of the tumor or to cells from normal, healthy tissue. These observations suggest that GlaS may provide an opportunity to target the enhanced PS on the outside of the CSCs for directed delivery to the cytoplasm of these cells. This would enable delivery of therapies (e.g. small molecules, radiation and/or biologics) directed at intracellular pathways into CSCs and limiting their off-target effects.

AnnV and Bavi are well known proteins used to bind PS. AnnV is commonly used to identify cells undergoing apoptosis, by specifically targeting PS due to loss of plasma membrane asymmetry[35]. Bavi is a mAb which acts as an immune modulating therapeutic, used to target PS exposed on the surface of tumor cells in the presence of β 2 glycoprotein (β2GPI)[36]. The antibody 11.31 (PGN632) is another PS-targeting mAb which does not require the presence of β2GPI, and has direct binding to PS[37,38]. These three characterized PS-binding proteins were used to confirm our observations of GlaS binding to CD44+ breast CSC. GlaS was found on the same percentage of CD44+ cells as AnnV, Bavi and 11.31, validating that it binds externalized PS. However, these PS binding proteins

did not always appear bound to the same cells, as determined by flow cytometry and microscopy[12] suggesting there may be differences in binding requirements for each of these PS-binding proteins. The cellular localization of these labeled proteins was examined using confocal microscopy, and only GlaS appeared to be internalized into the PDX cells. AnnV and Bavi only appeared bound to the cell membrane. Since the fluorophores used in these studies are small molecules, similar in size to chemotherapeutic agents, our observations reveal an opportunity to deliver molecular payloads into CSC to target intracellular pathways such as those related to Ras and other oncogenes (reviewed in[39]). In contrast, Bavi bound to exposed PS but remained on the outer surface of cells which may be useful for immune modulation[20], but would not enable targeting of intracellular pathways.

CD44 expression has been identified in many solid malignancies and is a well-known marker of CSCs[40–43]. In breast cancer, CD44+ CSCs are shown to exhibit high tumorigenicity and the ability to establish tumor heterogeneity following transplantation into mice[43]. An increase in CD44 expression identified in cells cultured under hypoxia has been observed before in breast cancer cell lines[44–46] as well as other models of cancer including glioma[47,48], gastric[25] and ovarian[49]. In this study, we observed that CD44 expression in the GlaS^{high}small cells was sensitive to oxygen condition in which the cells were cultured. Although a marker of CSC after lineage depletion, CD44 is expressed on normal cells including lymphocytes, fibroblasts, and smooth muscle cells in both humans and mice[50] making it a complicated target for directed delivery to the CSC.

Typically, CSCs reside within hypoxic areas of the tumor and can be identified based on their size; small sized cells are considered to be the quiescent, slow cycling stem cells[51–53]. Further, smaller sized CSCs have been found to enhance tumorigenicity *in vivo*[54]. Our study found that GlaS better targeted the small CD44+ cells (GlaS^{high}small), and further, had enhanced targeting under hypoxic conditions. These findings have significant implications, suggesting that GlaS could serve as a therapeutic delivery tool to specifically target the challenging-to-treat CSCs residing in the hypoxic TME.

Difficulties in targeting and treating CSCs have led to tumor relapse and poor patient outcomes. In this study, we reveal the natural PS externalization on the CSCs which is enhanced under hypoxia and demonstrate intracellular delivery follow GlaS binding to PS. GlaS targeted CD44+ cells, with superior targeting of the small CD44+ population, which was likely the small, tumorigenic CSC residing in the hypoxic TME. In the future, GlaS can serve as a platform for a PS-mediated intracellular targeted therapeutic delivery to potentially treat all tumor CSCs in their native hypoxic regions .

Methods

Patient derived xenografts

Human patient derived xenografts (PDX)s[31–33] were obtained from Dr. Huiping Liu (Northwestern University). Cells were derived from human triple negative breast cancer. Previously, CD44+ lineage negative CSC were isolated and engineered to express luciferase2- and tdtomato (L2T) or

eGFP (L2G) using lentivirus transduction[31]. Five PDX lines were used, which included M1L2T, M2L2T, M3L2G, CTC205 (L2T) and CTC092 (L2T). Cells were expanded in NOD-scid gamma (NSG) mice, obtained from Jackson laboratories (age 6-8 weeks). Cells from frozen samples were resuspended in PBS, mixed 1:1 with Matrigel to a total volume of 50 µl, and were injected into the right lower mammary fat pad. Because tumors varied in growth rate (ready to harvest in 2-6 months), injections were staggered so that the tumors were ready around the same time. When cells were used in culture, they were maintained in HuMEC media (Fisher Sci, cat#12-752-010) with growth factors (bovine pituitary extract and HuMEC supplements, added as per manufacturers instructions), 5% FBS and 0.5% penicillin/streptomycin. Cells were incubated at 37°C, 5% CO_2 and 4% O_2 (hypoxic), 7% O_2 (physoxic) or 21% O_2 (hyperoxic). To collect cells, supernatant was set aside, plates were incubated with trypsin for 5 min at 37°C followed by gentle scraping. Plates were washed using PBS and added to supernatant to collect cell pellet by centrifugation.

Expression and Purification of GlaS protein and GlaS fluorescent conjugation

GlaS protein was expressed and purified as described[12]. For fluorescence conjugation, purified protein underwent centrifugal ultrafiltration, TCEP reduction and maleimide conjugation to AlexaFluor (AF)647. AF647 GlaS was analyzed using size-exclusion chromatography and UV-Vis.

Tumor digestion

Tumors were excised, minced into ~2 mm pieces and incubated in a digestion solution (100 U/ml DNAse I (Stem Cell, cat#7900), Collagenase/Hyaluronidase 1X (Stem Cell, cat#7912) in RPMI) for 60 min, on a shaker at 80 rpm in a humidified incubator at 37°C and 5% CO_2. Cells were then filtered through a 70 µm strainer using PBS to wash plate and filter. Cells were centrifuged for 5 mins at 300G, supernatant aspirated and resuspended in 2 ml ACK lysis buffer for 1 min. 9 ml PBS + 10% FBS was then added and suspension was centrifuged again. Cells were resuspended in PBS followed by a sample being used for cell counting and viability using the trypan blue assay (Countess automated cell counter; Invitrogen, CA USA).

Cells were seeded into three 75 mm flasks (n=3) at a confluency of with $3x10^6$-$10x10^6$ cells total, depending on total number collected from tumors. One flask from each cell line was incubated at 4%, 7% or 21% O_2 at 37°C and 5% CO_2 overnight (~20 hours).

Flow cytometry

After overnight incubation in prescribed oxygen levels, cells were collected by supernatant, trypsinization, scraping and washing with PBS. All collection and staining procedures were performed in the appropriate oxygen condition. Cells were centrifuged at 300G for 5 mins when they were counted for staining. $1x10^6$ cells were seeded into a 96-well round bottom plate. All staining steps were performed in 100 µL volume in the dark. Samples were first incubated with Zombie NIR viability dye (1:750, BioLegend) for 30 min. Cells were washed once with flow buffer, followed by incubation with TruStain FcX PLUS (anti-mouse CD16/32) Antibody (BioLegend, Cat#156603; 0.25 µg/sample) and Human TruStain FcX (BioLegend, Cat#422301; 5 µl/sample) for

10 min. AF647 GlaS (1 µg/sample), PerCP CD44 (BioLegend, Cat#103035; 0.125 µg/sample) and AF594 Bavi or 11.31 antibodies (Birge Lab, Rutgers), each at 1 µg/sample, were then added and incubated for 30 min at room temperature. Bavi and 11.31 were used as PS-binding controls and stained with Alexa Fluor™ 594 Microscale Protein Labeling Kit (ThermoFisher, cat#A30008). Cells were washed twice with flow buffer prior to staining with BV421 Annexin V (BioLegend, Cat#141703; 2.5 µl/sample) in Annexin binding buffer (BioLegend, Cat#422201). Cells were washed twice with flow staining buffer and fixed with 4% PFA for 10 min and resuspended in a final volume of 100 µL for flow cytometry analysis using the Cytek Aurora spectral flow cytometer (Cytek, CA, USA). Single stained controls and unstained controls for all conditions were used to assess fluorescent spread and for gating strategies. Flow cytometry data was analyzed with the software FCSExpress (DeNovo Software, CA, USA). The data presented herein were obtained using instrumentation in the MSU Flow Cytometry Core Facility. The facility is funded in part through the financial support of Michigan State University's Office of Research & Innovation, College of Osteopathic Medicine, and College of Human Medicine.

Stastical Analysis

Statistics were performed using PRISM software (GraphPad, MA, USA; software version 9.0.0). Data is presented as mean +/- standard deviation (sdev). Staining from hypoxic, physoxic and hyperoxic conditions were compared using a one-way ANOVA with Tukey's multiple comparisons test. Equal variances were tested using Brown-Forsythe test and normal distribution was tested using Shapiro-Wilk test. If data failed the equal variances test, a Welch's ANOVA test with Dunnet's T3 multiple comparisons test was performed. If data failed the normality test, the non parametric Kruskal-Wallis with Dunn's multiple comparisons test was performed. Staining from $GlaS^{high}$small and $GlaS^{low}$large cells were compared using a two-tailed unpaired t test. If the data failed the D'Agostino & Pearson normality test, a nonparametric two-tailed Mann-Whitney test was performed. If the data did not have equal variances (F test), an unpaired two-tailed t test with Welch's correction was performed. A finding of $p<.05$ was considered significant.

Microscopy

M1L2T cells dissociated from a tumor were placed into hypoxic conditions overnight. Cells were then incubated with AF647 GlaS, BV421 AnnV and AF594 Bavi for 30 mins at room temperature. Cells were washed twice with staining buffer prior to fixation using 4% PFA for 10 min. A sample of 200,000 cells were spun onto a slide using a cytospin followed by placement of a coverslip for imaging. Imaging was performed using the Leica TCS SP8 X spectral upright confocal microscope system. Voxel size (x,y,z): 0.17 x 0.17 x 0.5 μm^3. Images were prepared using Fiji software (ImageJ; V2.9.0)[55].

Author contributions

AVM, CHC, TT and HL conceptualized the study. AVM performed experiments, data analysis and statistics. AVM, TT, TH and CHC contributed to the analysis and/or interpretation of the data. AVM drafted the manuscript. All authors critically revised and edited the manuscript.

Acknowledgements

We thank the MSU Flow Cytometry Core for their assistance in experimental planning, acquisition and analysis. We also thank the IQ Microscopy Core for their assistance in confocal microscopy training and help with acquisition.

References

1. Shiozawa, Y., Nie, B., Pienta, K. J., Morgan, T. M. & Taichman, R. S. Cancer stem cells and their role in metastasis. *Pharmacol Ther* **138**, 285–293 (2013).
2. Singh, S. K. *et al.* Identification of human brain tumour initiating cells. *Nature* **432**, 396–401 (2004).
3. Al-Hajj, M., Wicha, M. S., Benito-Hernandez, A., Morrison, S. J. & Clarke, M. F. Prospective identification of tumorigenic breast cancer cells. *Proceedings of the National Academy of Sciences* **100**, 3983–3988 (2003).
4. Lapidot, T. *et al.* A cell initiating human acute myeloid leukaemia after transplantation into SCID mice. *Nature* **367**, 645–648 (1994).
5. Soltanian, S. & Matin, M. M. Cancer stem cells and cancer therapy. *Tumor Biology* **32**, 425–440 (2011).
6. Yang, L. *et al.* Targeting cancer stem cell pathways for cancer therapy. *Signal Transduct Target Ther* **5**, 8 (2020).
7. Hankins, H. M., Baldridge, R. D., Xu, P. & Graham, T. R. Role of flippases, scramblases and transfer proteins in phosphatidylserine subcellular distribution. *Traffic* **16**, 35–47 (2015).
8. Fadok, V. A. *et al.* Exposure of phosphatidylserine on the surface of apoptotic lymphocytes triggers specific recognition and removal by macrophages. *J Immunol* **148**, 2207–2216 (1992).
9. Srivasatava, K. R., Majumder, R., Kane, W. H., Quinn-Allen, M. A. & Lentz, B. R. Phosphatidylserine and FVa regulate FXa structure. *Biochemical Journal* **459**, 229–239 (2014).
10. Riedl, S. *et al.* In search of a novel target—Phosphatidylserine exposed by non-apoptotic tumor cells and metastases of malignancies with poor treatment efficacy. *Biochimica et Biophysica Acta (BBA)-Biomembranes* **1808**, 2638–2645 (2011).
11. Vallabhapurapu, S. D. *et al.* Variation in human cancer cell external phosphatidylserine is regulated by flippase activity and intracellular calcium. *Oncotarget* **6**, 34375 (2015).
12. Hardy, J. *et al.* Gla-domain mediated targeting of externalized phosphatidylserine for intracellular delivery. *The FASEB Journal* **37**, e23113 (2023).
13. Jaiswal, S. *et al.* CD47 is upregulated on circulating hematopoietic stem cells and leukemia cells to avoid phagocytosis. *Cell* **138**, 271–285 (2009).
14. Riedl, S. *et al.* In search of a novel target—Phosphatidylserine exposed by non-apoptotic tumor cells and metastases of malignancies with poor treatment efficacy. *Biochimica et Biophysica Acta (BBA)-Biomembranes* **1808**, 2638–2645 (2011).
15. Birge, R. B. *et al.* Phosphatidylserine is a global immunosuppressive signal in efferocytosis, infectious disease, and cancer. *Cell Death Differ* **23**, 962–978 (2016).
16. Wang, W. *et al.* Mobilizing phospholipids on tumor plasma membrane implicates phosphatidylserine externalization blockade for cancer immunotherapy. *Cell Rep* **41**, (2022).
17. Van Rite, B. D. & Harrison, R. G. Annexin V-targeted enzyme prodrug therapy using cytosine deaminase in combination with 5-fluorocytosine. *Cancer Lett* **307**, 53–61 (2011).

18. Guillen, K. P., Ruben, E. A., Virani, N. & Harrison, R. G. Annexin-directed β-glucuronidase for the targeted treatment of solid tumors. *Protein Engineering, Design and Selection* **30**, 85–94 (2017).
19. Gerber, D. E. *et al. Tumor-specific targeting by Bavituximab, a phosphatidylserine-targeting monoclonal antibody with vascular targeting and immune modulating properties, in lung cancer xenografts*. *Am J Nucl Med Mol Imaging* vol. 5 www.ajnmmi.us/ (2015).
20. Yin, Y., Huang, X., Lynn, K. D. & Thorpe, P. E. Phosphatidylserine-targeting antibody induces M1 macrophage polarization and promotes myeloid-derived suppressor cell differentiation. *Cancer Immunol Res* **1**, 256–268 (2013).
21. Hardy, J. *et al.* Gla-domain mediated targeting of externalized phosphatidylserine for intracellular delivery. *bioRxiv* 2022.06.13.495901 (2022) doi:10.1101/2022.06.13.495901.
22. McKeown, S. R. Defining normoxia, physoxia and hypoxia in tumours—implications for treatment response. *Br J Radiol* **87**, 20130676 (2014).
23. Mas-Bargues, C. *et al.* Relevance of Oxygen Concentration in Stem Cell Culture for Regenerative Medicine. *Int J Mol Sci* **20**, (2019).
24. Heddleston, J. M., Li, Z., McLendon, R. E., Hjelmeland, A. B. & Rich, J. N. The hypoxic microenvironment maintains glioblastoma stem cells and promotes reprogramming towards a cancer stem cell phenotype. *Cell cycle* **8**, 3274–3284 (2009).
25. Liang, G. *et al.* Hypoxia regulates CD44 expression via hypoxia-inducible factor-1α in human gastric cancer cells. *Oncol Lett* **13**, 967–972 (2017).
26. Holmquist-Mengelbier, L. *et al.* Recruitment of HIF-1a; and HIF-2a; to common target genes is differentially regulated in neuroblastoma: HIF-2a; promotes an aggressive phenotype. *Cancer Cell* **10**, 413–423 (2006).
27. Bhaskara, V. K., Mohanam, I., Rao, J. S. & Mohanam, S. Intermittent hypoxia regulates stem-like characteristics and differentiation of neuroblastoma cells. *PLoS One* **7**, e30905 (2012).
28. Lendeckel, U. & Wolke, C. Redox-Regulation in Cancer Stem Cells. *Biomedicines* **10**, (2022).
29. Heddleston, J. M., Li, Z., McLendon, R. E., Hjelmeland, A. B. & Rich, J. N. The hypoxic microenvironment maintains glioblastoma stem cells and promotes reprogramming towards a cancer stem cell phenotype. *Cell cycle* **8**, 3274–3284 (2009).
30. Nascimento-Filho, C. H. V *et al.* From Tissue Physoxia to Cancer Hypoxia, Cost-Effective Methods to Study Tissue-Specific O2 Levels in Cellular Biology. *Int J Mol Sci* **23**, 5633 (2022).
31. Liu, H. *et al.* Cancer stem cells from human breast tumors are involved in spontaneous metastases in orthotopic mouse models. *Proceedings of the National Academy of Sciences* **107**, 18115–18120 (2010).
32. Tsai, C.-F. *et al.* Surfactant-assisted one-pot sample preparation for label-free single-cell proteomics. *Commun Biol* **4**, 265 (2021).
33. Dashzeveg, N. K. *et al.* Dynamic glycoprotein hyposialylation promotes chemotherapy evasion and metastatic seeding of quiescent circulating tumor cell clusters in breast cancer. *Cancer Discov* CD-22 (2023).

34. Ran, S. & Thorpe, P. E. Phosphatidylserine is a marker of tumor vasculature and a potential target for cancer imaging and therapy. *International Journal of Radiation Oncology*Biology*Physics* **54**, 1479–1484 (2002).
35. Vermes, I., Haanen, C., Steffens-Nakken, H. & Reutellingsperger, C. A novel assay for apoptosis flow cytometric detection of phosphatidylserine expression on early apoptotic cells using fluorescein labelled annexin V. *J Immunol Methods* **184**, 39–51 (1995).
36. Soares, M. M., King, S. W. & Thorpe, P. E. Targeting inside-out phosphatidylserine as a therapeutic strategy for viral diseases. *Nat Med* **14**, 1357–1362 (2008).
37. Moody, M. A. *et al.* Anti-phospholipid human monoclonal antibodies inhibit CCR5-tropic HIV-1 and induce β-chemokines. *Journal of Experimental Medicine* **207**, 763–776 (2010).
38. Calianese, D. *et al.* Phosphatidylserine-Targeting Monoclonal Antibodies Exhibit Distinct Biochemical and Cellular Effects on Anti-CD3/CD28–Stimulated T Cell IFN-γ and TNF-α Production. *The Journal of Immunology* **207**, 436–448 (2021).
39. Yang, L. *et al.* Targeting cancer stem cell pathways for cancer therapy. *Signal Transduct Target Ther* **5**, 8 (2020).
40. Schatton, T. *et al.* Identification of cells initiating human melanomas. *Nature* **451**, 345–349 (2008).
41. Hermann, P. C. *et al.* Distinct populations of cancer stem cells determine tumor growth and metastatic activity in human pancreatic cancer. *Cell Stem Cell* **1**, 313–323 (2007).
42. Galli, R. *et al.* Isolation and characterization of tumorigenic, stem-like neural precursors from human glioblastoma. *Cancer Res* **64**, 7011–7021 (2004).
43. Al-Hajj, M., Wicha, M. S., Benito-Hernandez, A., Morrison, S. J. & Clarke, M. F. Prospective identification of tumorigenic breast cancer cells. *Proceedings of the National Academy of Sciences* **100**, 3983–3988 (2003).
44. Krishnamachary, B. *et al.* Hypoxia regulates CD44 and its variant isoforms through HIF-1α in triple negative breast cancer. (2012).
45. Louie, E. *et al.* Identification of a stem-like cell population by exposing metastatic breast cancer cell lines to repetitive cycles of hypoxia and reoxygenation. *Breast Cancer Research* **12**, 1–14 (2010).
46. Bai, J. *et al.* HIF-2α regulates CD44 to promote cancer stem cell activation in triple-negative breast cancer via PI3K/AKT/mTOR signaling. *World J Stem Cells* **12**, 87 (2020).
47. Nishikawa, M. *et al.* Hypoxia-induced phenotypic transition from highly invasive to less invasive tumors in glioma stem-like cells: Significance of CD44 and osteopontin as therapeutic targets in glioblastoma. *Transl Oncol* **14**, 101137 (2021).
48. Pietras, A. *et al.* Osteopontin-CD44 signaling in the glioma perivascular niche enhances cancer stem cell phenotypes and promotes aggressive tumor growth. *Cell Stem Cell* **14**, 357–369 (2014).
49. Liang, D. *et al.* The hypoxic microenvironment upgrades stem-like properties of ovarian cancer cells. *BMC Cancer* **12**, 201 (2012).
50. Weng, X., Maxwell-Warburton, S., Hasib, A., Ma, L. & Kang, L. The membrane receptor CD44: novel insights into metabolism. *Trends in Endocrinology & Metabolism* **33**, 318–332 (2022).
51. De Paiva, C. S., Pflugfelder, S. C. & Li, D.-Q. Cell Size Correlates with Phenotype and Proliferative Capacity in Human Corneal Epithelial Cells. *Stem Cells* **24**, 368–375 (2006).

52. Li, Q., Rycaj, K., Chen, X. & Tang, D. G. Cancer stem cells and cell size: A causal link? in *Seminars in cancer biology* vol. 35 191–199 (Elsevier, 2015).
53. Son, S. *et al.* Direct observation of mammalian cell growth and size regulation. *Nat Methods* **9**, 910–912 (2012).
54. Li, H., Chen, X., Calhoun-Davis, T., Claypool, K. & Tang, D. G. PC3 Human Prostate Carcinoma Cell Holoclones Contain Self-renewing Tumor-Initiating Cells. *Cancer Res* **68**, 1820–1825 (2008).
55. Schindelin, J. *et al.* Fiji: an open-source platform for biological-image analysis. *Nat Methods* **9**, 676–682 (2012).